BIOCHEMISTRY
including biophysical chemistry & molecular biology

ARTICLE

pubs.acs.org/biochemistry

Natural Osmolytes Remodel the Aggregation Pathway of Mutant Huntingtin Exon 1

Tejas Borwankar,[†] Christoph Röthlein,[†] Gong Zhang,[†] Anne Techen,[‡] Carsten Dosche,[‡] and Zoya Ignatova*[,†]

[†]Department of Biochemistry, Institute of Biochemistry and Biology, and [‡]Department of Physical Chemistry, Insitute of Chemistry, University of Potsdam, Karl-Liebknecht-Strasse 24-25, 14467 Potsdam, Germany

Supporting Information

ABSTRACT: In response to stress small organic compounds termed osmolytes are ubiquitously accumulated in all cell types to regulate the intracellular solvent quality and to counteract the deleterious effect on the stability and function of cellular proteins. Given the evidence that destabilization of the native state of a protein either by mutation or by environmental changes triggers the aggregation in the neurodegenerative pathologies, the modulation of the intracellular solute composition with osmolytes is an attractive strategy to stabilize an aggregating protein. Here we report the effect of three natural osmolytes on the *in vivo* and *in vitro* aggregation landscape of huntingtin exon 1 implicated in the Huntington's disease. Trimethylamine *N*-oxide (TMAO) and proline redirect amyloid fibrillogenesis of the pathological huntingtin exon 1 to nonamyloidogenic amorphous assemblies via two dissimilar molecular mechanisms. TMAO causes a rapid formation of bulky amorphous aggregates with minimally exposed surface area, whereas proline solubilizes the monomer and suppresses the accumulation of early transient aggregates. Conversely, glycine−betaine enhances fibrillization in a fashion reminiscent of the genesis of functional amyloids. Strikingly, none of the natural osmolytes can completely abrogate the aggregate formation; however, they redirect the amyloidogenesis into alternative, nontoxic aggregate species. Our study reveals new insights into the complex interactions of osmoprotectants with polyQ aggregates.

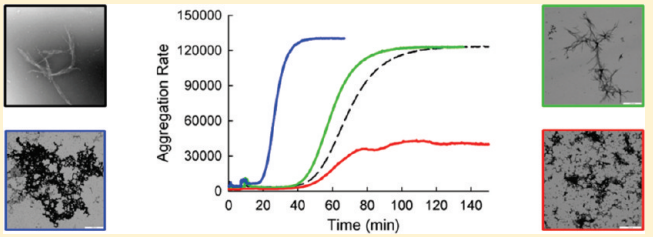

Osmotic or thermal stress leads to fluctuations in the cell volume and solute composition in the cytosol which can, in turn, severely alter the stability of the cellular protein bulk.[1] A basic stress response in living systems is to maintain protein stability by regulating solvent quality[2] while cell volume is retained by carefully controlled adjustment of the concentration of compatible osmolytes, small organic molecules that regulate the solvent quality.[3,4] Osmolytes markedly influence the protein folding reaction: protecting osmolytes (also called osmoprotectants and chemical chaperones) shift the equilibrium toward the native state, whereas denaturing osmolytes (e.g., urea) shift the equilibrium to the unfolded state.[5] Protecting osmolytes thermodynamically stabilize proteins by repopulating the denatured and native states via unfavorable interactions with protein surfaces (a combination of backbone and side-chain interactions).[2] The statistical mechanics backbone solvation theory frames the osmolytes action into a universal molecular mechanism and suggests that backbone/osmolyte interaction energy depends on the osmolyte polarity (i.e., different energies are released from interactions of the protein backbone with polar and nonpolar osmolyte areas) and interaction degeneracy (i.e., energetically equivalent possibilities to establish interactions) which is a function of the osmolyte surface area.[5] Cells have evolved elaborate mechanisms to detect protein damage induced by volume changes vs protein destabilization by other types of external (e.g., thermal) stress: Signaling pathways controlling the osmocompensatory response are specifically induced by damage to proteins undergoing *de novo* synthesis.[6] Protecting osmolytes can be either synthesized endogenously or taken up from the external cellular milieu through transporters[7] and accumulate in cells at a high concentration (>0.4 M)[8,9] without interfering with protein function or metabolic activities.[4]

In a variety of neuropathologies, including Huntington's disease and several ataxias, the corresponding disease proteins self-assemble into discernible inclusions containing morphologically similar, detergent-resistant fibrillar amyloids. A distinctive feature of these proteins which have otherwise dissimilar primary sequences is the presence of an unstable homopolymeric polyglutamine (polyQ) tract with repeat length over a pathological threshold value of 30−40 glutamines that inversely correlates with disease penetrance, severity, and age of onset.[10] This observation led to the suggestion that polyQ expansion is the

Received: November 17, 2010
Revised: February 4, 2011
Published: February 07, 2011

aggregation-triggering event in polyQ diseases (also known as CAG-repeat disorders). In addition to the amyloid fibrils, however, small oligomeric or protofibrillar aggregates are accessible to the polyQ proteins[11] in which sequences outside the polyQ stretch interact to transiently form the aggregate core.[12] The crowded environment, the plethora of other proteins, small ligands, and posttranslational modifications in the cell can influence the appearance and formation of aggregates *in vivo*.. Various cellular proteins, e.g., heat shock proteins, alter the morphology and cytotoxicity of the aggregate species,[13,14] suggesting that the aggregation of polyQ-containing proteins *in vivo*. is far more complex than under defined conditions *in vitro*. Physicochemical properties of the cellular environment change as a consequence of external stress (i.e., aging, osmotic, oxidative stress) and markedly accelerate the aggregation of polyQ proteins.[15−18] However, the molecular mechanisms by which cellular environment modulates aggregation pathways remain a fundamentally unresolved issue.

The assembly into amyloid fibrils is accompanied by conformational changes in the aggregating proteins. In the polyQ pathology the aggregation propensity of the disease proteins is a result of interplay between the polyQ stretch and the sequences flanking them (refs 12, 19, and 20 and references cited therein). The polyQ stretch destabilizes the host sequence in a polyQ repeat length-dependent fashion[21,22] and enhances the aggregation propensity of the entire protein;[12] this raises the intriguing hypothesis of whether the natural osmocompensatory response can be employed to counteract the destabilization effect of the polyQ expansion mutation and ameliorate polyQ pathologies.

The molecular mode of action of the protective osmolytes can be rationalized by combination of preferential exclusion of the solutes from the peptide backbone and favorable/unfavorable interactions with the amino acid side chains.[23] Given that several species with different morphologies (i.e., nucleus, oligomers, protofibrils, and fibrillar amyloids) and consequently with various protein surfaces (a combination of the exposed backbone and side-chains) are accessible in the polyQ aggregation, it raises the question as to whether osmolytes exert different effects on each of these species. Isolated examples show that some osmolytes (trehalose and ectoine) alleviate polyQ-mediated pathologies: their effect however ranges from reducing the aggregate formation[24] to altering their subcellular localization[25] and to enhancing the mTOR-independent autophagy that accelerates the clearance of polyQ aggregates.[26] Variations in the interpretations of the osmolyte effect emphasize the need for careful systematic analysis of the impact of osmolytes on the polyQ aggregation. Here, we have undertaken a systematic structural analysis to address the impact of various osmolytes on the *in vivo* and *in vitro* aggregation landscape of huntingtin exon 1 (Htt) with pathological expansion of the polyQ tract. Intriguingly, we observed that proline and TMAO induced nonamyloidogenic and nontoxic amorphous aggregates, employing two different molecular mechanisms. TMAO, the most effective osmoprotectant, quickly precipitated out the Htt53Q monomer forming bulky, detergent-resistant aggregates. Proline solubilized the monomer and induced formation of small amorphous, but detergent-labile assemblies. By contrast, GB enhanced the fibril formation in a fashion reminiscent of the growth of the nontoxic functional amyloids, and although resembling characteristic features of amyloid structures, the aggregates exerted no toxic effect on neroblastoma N2a cells. These findings reconcile conflicting reports on the role of osmolytes in amyloidogenesis and define new parameters to couple the stress response to modulate aggregation pathways.

EXPERIMENTAL PROCEDURES

In-Cell FRAP Experiments. DNA fragments encoding N-terminal GFP fusions of Htt exon 1 with 25Q or 53Q were cloned into a pET-16b (Amp^r, Ptac, lacI; Pharmacia) vector and expressed in *Escherichia coli* BL21(DE3) (*ompT hsdS dcm*$^+$ Tet^r *gal*(DE3) *end*A Hte; Stratagene). Until the midexponential phase (OD_{600} = 0.4) cells were grown in LB medium containing ampicillin (100 μg/mL) as a selection marker at 37 °C and then transferred into a minimal medium,[27] and the expression of the protein was induced by adding 0.6 mM isopropyl β-D-thiogalactoside (IPTG). NaCl (300 mM) was added to some aliquots to exert osmotic stress. To initiate the osmolyte uptake, 20 mM osmolytes (proline or GB) were added to some aliquots simultaneously with 300 mM NaCl, and cells were analyzed usually at 210 min after induction of the Htt53Q aggregation. A 4 μL bacterial suspension was placed on a concanavalin A precoated glass slide and processed on an Applied Precission DeltaVision RT System (100× immersion objective, NA 1.25; laser beam 0.8 μm). Three prebleach images were recorded; the sample was then fired with a single 100 ms bleach pulse with 20% laser power, and images with exposure time of 0.05 s/frame were recorded. The intensity of each image was normalized to relative intensity (RI) as established for in-cell FRAP analysis:[14,28,29] $RI_{t=i} = (I_i/I_{nbi})/(I_0/I_{pb})$, where I_i and I_{nbi} are the integrated intensities of the bleached and nonbleached area at any given time point and I_0 and I_{pb} are the integrated intensities before photobleaching of the bleached and nonbleached area, respectively. The software for calculating the fluorescence intensities of the FRAP images was written in Visual BASIC.NET. The relative intensity values were plotted against the time and fit in Sigma Plot using standard three- or five-parameter exponential functions. The mobile fraction (M_f) was determined using the equation $M_f = (I_{i,final} - I_0)/(I_1 - I_0)$, where $I_{i,final}$ is the averaged final intensity after full recovery and I_1 is the averaged intensity of the first image recorded after photobleaching.

Protein Expression and Purification. For *in vitro* experiments full-length Htt exon 1 with 20Q or 53Q was cloned into a pGEX-6P plasmid (GE Healthcare) downstream of the GST and PreScission protease moiety. *E. coli* BL21(DE3) cells transformed with either of the plasmids were cultured at 37 °C in LB medium containing ampicillin. At $OD_{600} \sim 0.4$ protein expression was induced by adding 0.6 mM IPTG, and the cells were further cultivated for 6 h at 30 °C. GST-Htt proteins were purified from the soluble cell extract on a GST-Sepharose 4 Fast-Flow (GE Healthcare), dialyzed in 50 mM Tris-HCl buffer (pH 8.0), 150 mM KCl, and 10% (v/v) glycerol, flash frozen in liquid nitrogen, and stored in aliquots at −80 °C. The concentration of the stocks was determined using the Bradford method. For aggregation analysis the buffer of the frozen aliquots of GST-Htt20Q and GST-Htt53Q was exchanged to 50 mM Tris-HCl (pH 7.5) containing 150 mM NaCl, 1 mM EDTA, and 1 mM DTT by dialysis at 4 °C.

***In Vitro* Aggregation and Aggregate Analyses.** *(i) Filter-Retardation Assay.* Aggregation kinetics of 5 μM pure GST-Htt20Q and GST-Htt53Q at 30 °C was monitored by filter-retardation assay as described.[30] Osmolytes at 0.5 M were added together with the PreScission protease (GE Healthcare) that releases the GST moiety and initiates aggregation. At different time points samples were withdrawn, supplemented with 2% SDS, heated 5 min at 95 °C, and loaded onto cellulose acetate membrane (0.2 μm pore size) using a slot-blot manifold (Hoefer): The membranes were developed with MW8 antibody[31] in 1:200

dilution. Only SDS-resistant species were retained on the membrane. Subsequently, the membranes were developed with a peroxidase conjugate of anti-mouse IgG antibody at 1:1000 dilution and visualized with Rodeo ECL Western blotting reagent (USB Corp., Germany) and recorded on a Fuji-Imager (LAS-3000) instrument. The intensity of the spots was quantified using ONE-Dscan (Scananalytics, CSPI, USA). In the time-based filter-retardation assays the intensity of the spots at each time point (I_i) was converted into relative intensity ($I_{i,r}$) using the equation $I_{i,r} = (I_i - I_0)/(I_{end} - I_0)$, where I_0 is the intensity at the start of the reaction and I_{end} is the intensity of the end sample. Note that direct comparison of the absolute intensities among different filter-retardation assays is not possible.[32] To compare the time course of kinetics among different experiments for each independent time experiment, the slot with the highest signal intensity was arbitrarily set as 1 as previously established.[32]

(ii) Thermal Depolymerization. The completely aggregated samples of 5 μM Htt53Q grown with and without osmolytes were incubated at increasing temperatures (25−95 °C in 10 °C intervals) for 5 min in 1.6% SDS followed by SDS−PAGE separation[33,34] and immunoblot analysis using MW1 antibody which recognizes monomers preferably.[35] The total recoverable monomer from the control Htt53Q fibrils was determined by boiling the samples at 95 °C for 5 min and using as loading control. The intensity of the band of interest on the immunoblots was quantified using ONE-Dscan (Scananalytics, CSPI, USA), and the intensity of each experiment was normalized to the intensity of the monomer band of the loading control.

(iii) Light Scattering. The aggregation kinetics of 5 μM Htt proteins with or without osmolytes at different end concentrations were monitored by static light scattering at 30 °C at 532 nm as described elesewhere.[36] The curves were fit to four-parameter sigmoidal equations, and the processing software was SigmaPlot.

(iv) Analytical Size-Exclusion Chromatography. Intact aggregates from the *E. coli* expressing cells were isolated as described[37] and separated on a Sephadex G-200 column at a flow rate of 0.1 mL/min in 50 mM Tris-HCl, pH 7.0, containing 150 mM NaCl. The collected fractions (200 μL) were split and loaded onto nitrocellulose membrane that retains the detergent-labile species and on cellulose acetate membrane, i.e., filter-retardation assay for SDS-insoluble fractions.[30] Before being loaded onto the column cell lysates were centrifuged briefly (500*g* for 3 min) to remove cell debris. The column was calibrated with protein standards (high molecular weight gel filtration calibration kit; GE Healthcare).

(v) Electron Microscopy. Samples (5 μL) were withdrawn from ongoing aggregation reactions, stained with 2% (w/v) uranyl acetate, and viewed on an EM 902 transmission electron microscope (Zeiss).

Seeding Experiments. Aggregates of Htt53Q were grown *in vitro* in the presence or absence of osmolytes overnight to allow complete aggregation and then sonicated on ice for 5 s in 1 s bursts and 20% output (HTU SONI130 sonifier; Heinemann). Ten percent (w/w) of the preformed seeds were added to the new aggregation reactions of GST-Htt53Q together with the PreScission protease (GE Healthcare). The reaction was further monitored by filter-retardation assay. Similarly, seeding experiments were performed with *in vivo* formed Htt aggregates. *E. coli* cells expressing GFP-Htt53Q protein for 5 h were used to isolate intact cellular aggregates as previously described.[37]

FCS Measurements. To obtain a single cysteine-containing GST-Htt53Q and GST-Htt20Q, all cysteine residues within the GST counterpart were replaced by serine, and one cysteine upstream of the polyglutamine tract was introduced using the QuickChange protocol (Stratagene). The modified constructs were purified as described for the wild-type GST-Htt proteins. Five micromolar mutant constructs together with 20Q and 53Q were labeled with a 20-fold molar excess of Alexa-633 and a 10-fold excess of tris(2-carboxyethyl)phosphine (TCEP) solution for 3 h at 4 °C. The free dye was removed by size-exclusion chromatography on Micro-Bio-Spin 6 columns (Bio-Rad). For FCS measurements, the labeled stock was diluted to a final concentration of 5 nM in 10 mM Na_2HPO_4, pH 7.0, containing 120 mM NaCl and 1 mM EDTA, mixed with unlabeled GST-Htt53Q or GST-Htt20Q to a final concentration of 5 μM. The correlation curves were recorded on an inverse time-resolved, confocal microscope system (MicroTime 200 and Time Harp 200 OC-board; PicoQuant) with a high numeric aperture objective (Olympus Plan Apo, 100×, NA 1.4, oil immersion) and with an AOTF filtered output of a super-continuum white light source (SC 400-2; Fianium Ltd.) as excitation source (λ = 630 nm, 30 ps pulse width, repetition rate 20 MHz, dichroic mirror z467/638rpc, excitation power 70 μW). The emitted intensity fluctuations were transmitted through the dichroic mirror, passed through a 50 μm pinhole, and detected by two single-photon avalanche photodiodes (SPCM-AQR SPAPD; Perkin-Elmer) over a total measurement time of 20 min. The fluorescence intensity is given by the autocorrelation function ($G(\tau)$):[38]

$$G(\tau) = \frac{\langle \delta I(t) \delta I(t+\tau) \rangle}{\langle I(t) \rangle^2}$$

where the fluorescence intensity fluctuations $\delta I(t)$ at the time t and $\delta I(t+\tau)$ at a time delay τ are normalized by averaged mean fluorescence intensity over the time of measurement $\langle I(t) \rangle$. The intensity fluctuations $\delta I(t)$ can be expressed as $\delta I(t) = I(t) - \langle I(t) \rangle$. The cross-correlation function was calculated with the software SymPhoTime 4.9 (PicoQuant), and the focal volume was determined using Atto655 as a calibration standard. Some curves showed fluctuating traces for the slow components. Therefore, we first performed 13-point regression smoothing, followed by spline interpolation to homogenize the point distribution around in the noise area. Thereafter, the first derivative (G') was ascertained using MatLab software, and the curves representing the dependence of G' as a function of the dwell time of the fluorescent species in the confocal volume during the time course of the aggregation reaction were fit up to a three-component model using the Gaussian function; the Htt20Q was analyzed using a one-component fit. The amplitude of the G', i.e., the correlation between the intensity of the signal and the concentration of the species, might deviate from the ideal proportionality because some species may contain more than one fluorophore. The significance of the peaks was statistically assessed using the χ^2-square test.

RESULTS

Various PolyQ Aggregates Are Formed in the Cell. To explore the effect of natural osmoprotectants on the aggregation of polyQ-containing proteins, we first sought to establish a system for directly monitoring the behavior *in vivo*. We fused fragments of full-length exon 1 of huntingtin (Htt) with a polyQ tract either in the nonpathological (GFP-Htt25Q) or pathological

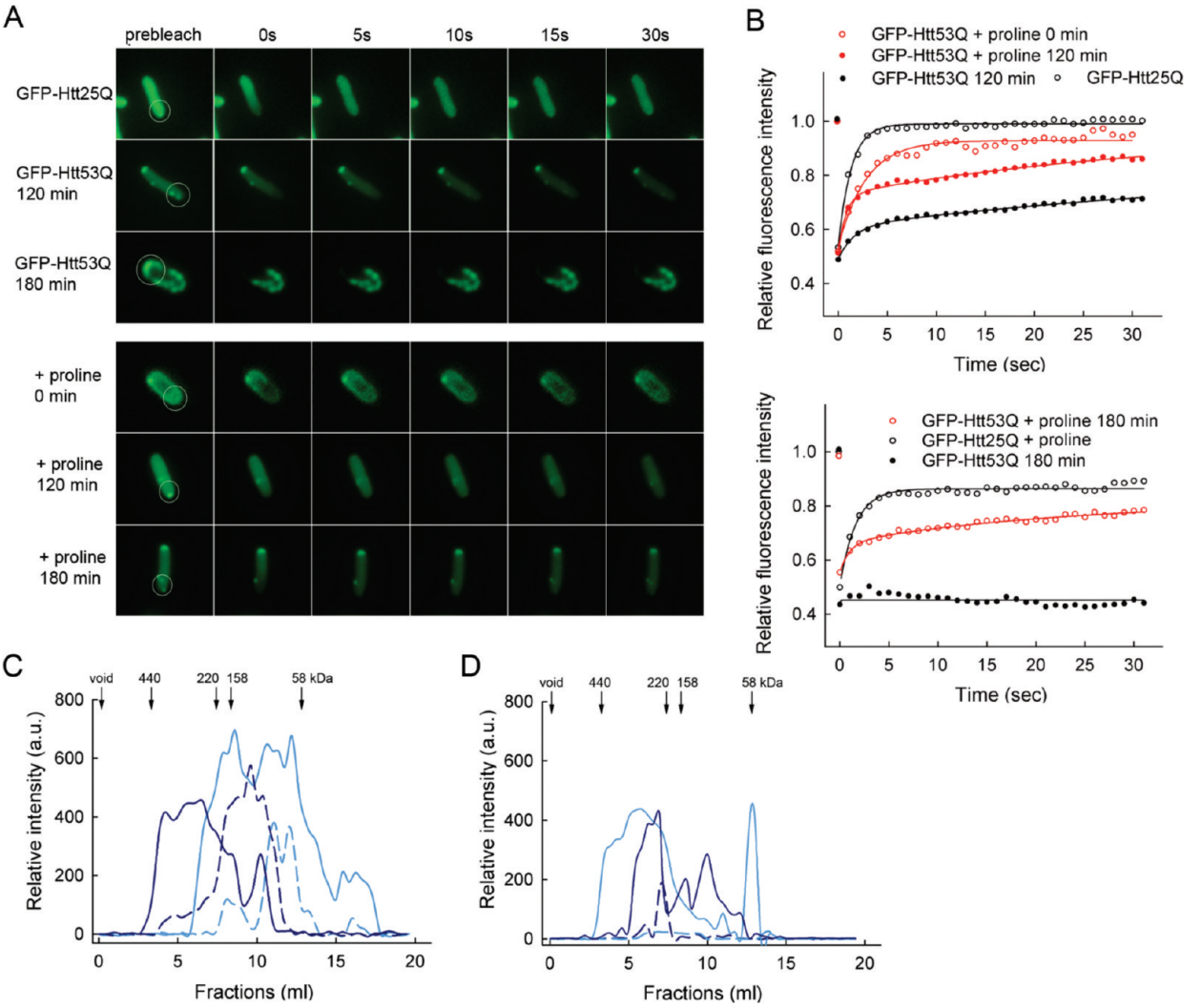

Figure 1. Proline inhibited the GFP-Htt53Q fibrillization *in vivo* and changed the physicochemical properties of the aggregates. (A) FRAP analysis of cellular GFP-Htt53Q aggregates in the absence (upper panel) and presence (bottom panel) of proline. Cells expressing GFP-Htt53Q were subjected to FRAP analysis at early (120 min) and later time points (180 min) after induction (times are indicated to the left of each image row, upper panel). The soluble GFP-Htt25Q protein showed complete recovery. Proline increased the recovery of GFP-Htt53Q aggregates in the cell (bottom panel) when internalized at various times of GFP-Htt53Q expression (times are indicted to the left of each image row). The white circle on the prebleach image marks the area of bleaching. (B) Quantitative analysis of the FRAP images. Fluorescence intensity in the bleached area of each FRAP image in panel A is converted into relative fluorescence intensity. Solid lines represent a curve fit to a three-parameter single exponential or a five-parameter double exponential function. The curve of GFP-Htt53Q 180 min yielded a very poor fit due to the very low recovery. (C) Detergent-resistant species appeared early in GFP-Htt53Q aggregation. Intact in-cell GFP-Htt53Q aggregates were isolated at early (light blue) and late (dark blue) stage and fractionated by size-exclusion chromatography into SDS-labile species (solid lane) and SDS-resistant species (dashed lane). (D) Proline suppressed the formation of detergent-resistant aggregates. Intact aggregates were isolated 210 min after induction of GFP-Htt53Q aggregation, and proline uptake was internalized at the time of induction (0 min, light blue) or at a later expression phase (180 min, dark blue). Solid and dashed lines represent the SDS-soluble and SDS-insoluble species, respectively. The numbers at the top of the plot denote molecular mass markers used to calibrate the column; "void" marks the void volume.

(GFP-Htt53Q) range onto the C-terminus of the green fluorescent protein (GFP). The GFP chimeras retained the polyQ length-dependent aggregation behavior characteristic of polyQ-dependent neuropathies[10] in the cellular system used here, namely, *E. coli*: GFP-Htt53Q aggregated in peripheral hyperfluorescent loci that were composed predominantly of SDS-resistant species, whereas the GFP-Htt25Q was soluble and uniformly distributed in the cytosol (Figure 1A, Supporting Information Figure S1). Detergent resistance recapitulates the important pathological hallmark of aggregates with fibrillar structures (preaggregates or mature fibrils) in Huntington's disease.[10,39] Although not a natural cellular environment for the polyQ pathologies, *E. coli* has been shown to support the formation of cellular aggregates that are structurally homologous to those formed in eukaryotic cells.[40] *E. coli* is a simple model cellular system and as a non-natural environment of the Htt pathology allows decoupling of the aggregation process from the cellular dysgenesis as a result of the cytotoxic effect of various aggregates. *E. coli* enables a precise tuning of its cellular environment, allowing the exploration of structural and biophysical aspects of interactions of small molecules (here osmolytes) with amyloidogenic systems in a crowded environment.

dx.doi.org/10.1021/bi1018368 |*Biochemistry* 2011, 50, 2048–2060

Table 1. Quantitative Analysis of GFP-Htt Mobility

protein	aggregation time and time of osmolyte internalization	mobile fraction[a] (%)
GFP-Htt25Q		81 ± 4.2
	+proline	85 ± 9.0
	+GB	87 ± 6.5
GFP-Htt53Q	120 min	40 ± 5.3
	180 min	5 ± 2.1
	+proline, 0 min	75 ± 14.0
	+proline, 120 min	62 ± 15.5
	+proline, 180 min	61 ± 15.5
	+GB, 0 min	52 ± 11.7
	+GB, 120 min	30 ± 5.8
	+GB, 180 min	9 ± 7.0

[a] The mobile fraction is calculated based on the FRAP analyses in Figures 1B and 4B. The standard deviation is a mean value of the analysis of five cells.

To compare the dynamic properties of the polyQ aggregates in the cell, we used fluorescence recovery after photobleaching (FRAP) which measures the diffusion and mobility of fluorescently tagged proteins in a defined compartment, here the *E. coli* cytoplasm.[28] Induction of expression of GFP-Htt53Q was used to initiate the aggregate formation (Supporting Information Figure S1), and recovery of the fluorescence was monitored after a pulse of photobleaching of a small area of the cell (Figure 1A). The mobility of the GFP-Htt53Q aggregates decreased in a time-dependent manner: at early time points (120 min) the fluorescence recovered to 40% whereas at late time points (180 min) the aggregates were completely immobile (Figure 1A,B), and mobility was reduced to 5% (Table 1). By comparison, the soluble GFP-Htt25Q was highly mobile, displaying immediate recovery after photobleaching (Figure 1A,B) with a mobility fraction of 81% (Table 1). Intriguingly, the recovery profile of the early stage aggregates of GFP-Htt53Q (120 min) showed an initial fast recovery phase followed by a slower, incomplete recovery (Figure 1B), suggesting the coexistence of two (or more) monomeric species with different mobility within the aggregates. We next isolated intact GFP-Htt53Q aggregates at different time points of expression and fractionated them by size-exclusion chromatography. Each eluted fraction was analyzed for detergent lability and detergent resistance. In the early phases of GFP-Htt53Q aggregation, SDS-labile and SDS-resistant species were coeluted (Figure 1C), which most likely accounts for the two phases in the recovery kinetics at 120 min (Figure 1B). At a later stage of aggregation (180 min) the amount of detergent-resistant aggregates increased (Figure 1C), paralleling the decrease of the fluorescence recovery (Figure 1B). The SDS-resistant species migrated slower than the detergent-labile aggregates, most likely due to their fibrillar structure.

Proline Inhibits PolyQ Fibrillization in the Cell. Increase in the osmolarity of the external medium induces the osmotic stress response in *E. coli* by rapidly activating the membrane ProP transporter, which actively takes up osmolytes from the nutrient medium.[7] The ProP transporter has a broad substrate specificity and can transport proline, GB, and ectoine.[27,41]The upregulation of only one type of osmolyte in the cytoplasm can be controlled using a medium with a defined composition supplied with this osmolyte; an osmoprotective substance already available in the nutrient medium has priority over the endogenously synthesized osmolytes (e.g., trehalose, glycerol) as it ensures more rapid osmoadaptation of the cells.[7] Concomitant with exposing the cells to osmotic upshift, we supplied the medium with 20 mM proline. The activation of ProP occurs within 20 s of upshock given that K^+ is also available in the nutrient medium.[9] Proline uptake is a rapid process, and a high proline concentration (>0.4 M) in the cytosol is established between 5 and 10 min after exposure to stress.[42] Proline accumulation in the cell did not influence the cell growth or protein expression level (Supporting Information Figure S2A−C). When proline was present throughout the aggregation reaction (added at 0 min), some hyperfluorescent loci consistent with aggregates were formed (Figure 1A), which, however, displayed relatively high mobility (75%, Table 1). In addition, their fluorescence recovery curve could be fit to a single exponential indicating that the aggregate comprised species of uniform mobility (Figure 1B, upper panel). The detergent-resistant structures accounting for fibrillar preaggregates or mature aggregates were completely suppressed as assessed by fractionation of the aggregates with size-exclusion chromatography (Figure 1D). Intriguingly, a new fraction that migrated with an apparent molecular mass of the GFP-Htt53Q monomer (~55 kDa) was enriched. Proline internalization at later time points (120 and 180 min), at which the GFP-Htt53Q partitioned between the detergent-labile and detergent-resistant fractions (Figure 1C), also increased aggregate mobility to 62% and 61%, respectively (Table 1). The kinetics of fluorescence recovery retained the double-exponential behavior (Figure 1A,B), suggesting that the aggregates consist of species with nonuniform mobility; however, the amount of SDS-resistant aggregates was markedly reduced (Figure 1D). In the later phases of aggregation, proline markedly suppressed further fibrillization but was not able to completely solubilize the existing SDS-resistant GFP-Htt53Q aggregates.

Proline Alters PolyQ Aggregation *in Vitro*. Next, we investigated the effect of proline on Htt53Q fibrillogenesis in *in vitro* experiments with Htt exon 1 with 53Q. Both GST-Htt20Q and GST-Htt53Q were purified by affinity chromatography to high homogeneity (Supporting Information Figure S2D). Note that during subcloning the nonpathological variant (Htt25Q) the polyQ stretch was shortened by five polyglutamine residues due to the high instability of the polyQ stretch. This shorter Htt20Q construct was soluble throughout the aggregation cycle (Figure 2A) and exhibited behavior identical to that of the GFP-Htt25Q protein used in the *in vivo* experiments. The aggregation of Htt53Q *in vitro* was initiated by adding PreScission protease which completely released the GST tag (Supporting Information Figure S3), and we monitored the process by static light

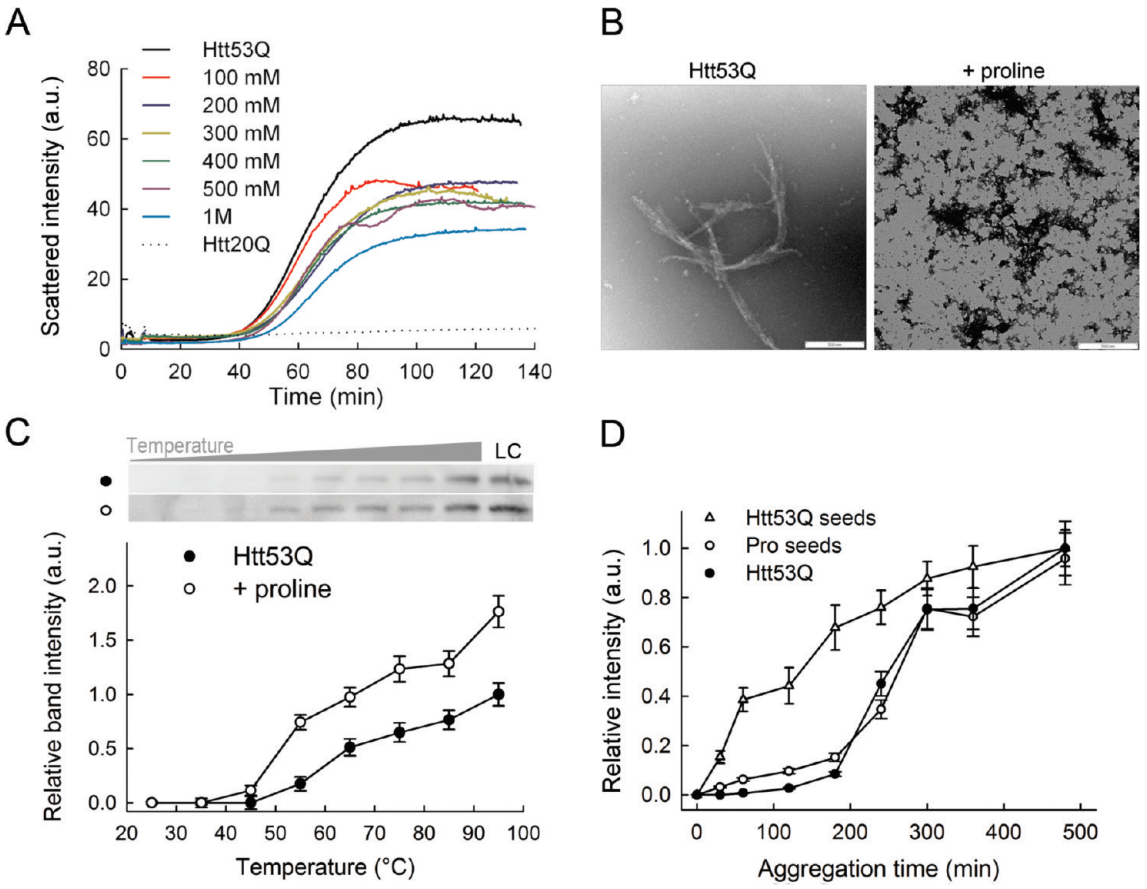

Figure 2. Proline altered the aggregation of Htt53Q *in vitro*. (A) Aggregation kinetics of Htt53Q in the absence and presence of various concentrations of proline were monitored by static light scattering. The soluble Htt20Q protein showed no change in the scattered light throughout the analysis. (B) Electron micrographs of the end-stage Htt53Q aggregates grown for 24 h in the absence and presence of 0.5 M proline. Scale bar = 500 nm; magnification 27000× for control and 20000× for proline. (C) Htt53Q aggregates assembled in the presence of 0.5 M proline showed higher susceptibility to thermal depolymerization and released higher amounts of monomer than the control Htt53Q fibrils. The amount of monomer released from the aggregates was related to the intensity of the loading control (LC; see Experimental Procedures section). (D) End-stage aggregates of Htt53Q grown *in vitro* in the presence of proline were unable to seed the Htt53Q elongation. Htt53Q fibrillization (5 μM) was seeded with 10% (w/w) aggregates grown with (Pro seeds) or without proline (Htt53Q seeds), and the aggregation kinetics was monitored by filter-retardation assay. Values represent means ± SD (n = 3).

scattering and thioflavin T (ThT) binding assay. The Htt53Q aggregation kinetics displayed a sigmoidal behavior with an initial lag-like phase of ~40 min (Figure 2A, Supporting Information Figure S4A); fibrillar structures were predominantly accessible at the end stage of aggregation (Figure 2B). In contrast, when proline was present throughout the aggregation reaction (added at 0 min) the lag-like phase was extended (Figure 2A), and the end intensity of the ThT signal was markedly reduced (Supporting Information Figure S4A). Proline induced formation of amorphous aggregates with no apparent fibrillar structure (Figure 2B), which showed an enhanced susceptibility to thermal depolymerization (i.e., enhanced release of the monomer) as opposed to the Htt53Q fibrillar aggregates (Figure 2C). When proline was added at a later phase of the Htt53Q aggregation (1 h), the ThT fluorescence signal reached a plateau (Supporting Information Figure S4A) suggesting that proline most likely suppressed further fibrillar growth. The addition of proline at a later stage of aggregation (1 and 3 h) led to slight decrease in the susceptibility of the aggregates to thermal depolymerization compared to the reaction in which proline was present throughout the aggregation reaction (0 h; Supporting Information Figure S4B). Thus, the impact of proline *in vitro* remarkably resembled the *in vivo* effect: proline reduced the fibril assembly in favor of amorphous protein when added at the initiation of the aggregation, whereas at later phases it inhibited further fibrillization.

In the *in vitro* experiments, our logic was to use predominantly 0.5 M proline since proline can be upregulated to similar concentrations in the *E. coli* cells.[42] For some organisms, however, other concentrations of the protecting osmolytes have been favored, probably dependent on the strength of external threat to which each cell is exposed.[43] Intriguingly, we observed only a slight concentration dependence of the proline effect on Htt53Q aggregation (Figure 2A).

To test whether proline changed the core of the aggregates, we used a complementary approach, the seeding ability, which is a sensitive and remarkably discriminating assay for exploring structural features of distinct aggregates.[37,44] The key feature of this approach is based on the ability of preformed aggregates or seeds to recruit new monomers with sequences identical to the aggregate core and thereby efficiently bypass the initial lag-like phase. The Htt53Q aggregates grown in presence of proline were seeding-incompetent and did not change the time course of Htt53Q aggregation *in vitro* (Figure 2D). Similarly, the GFP-Htt53Q aggregates isolated from cells with upregulated proline

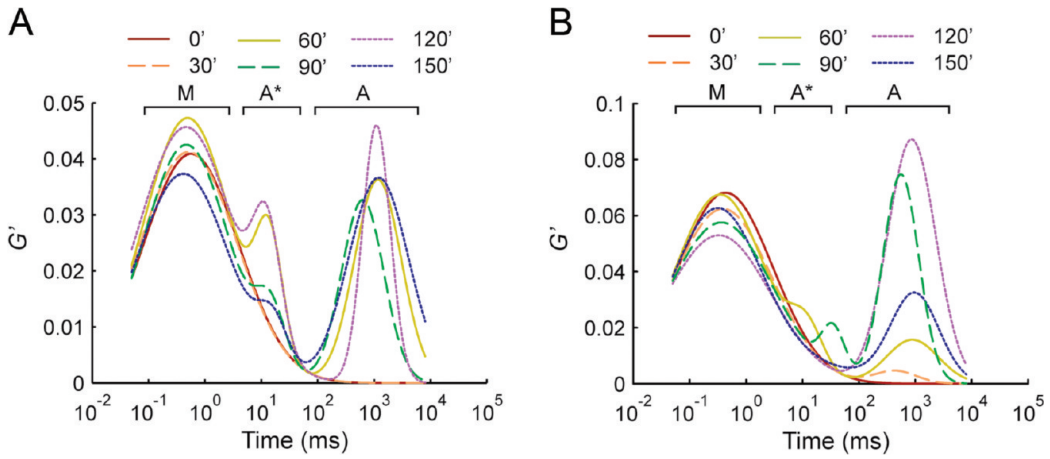

Figure 3. Proline changed the aggregation pattern of Htt53Q in the early phase. Time-dependent changes in the dwell times of the fluorescent particles in the confocal volume during the aggregation of Htt53Q in the absence (A) and in the presence (B) of proline. The three main peaks were selected as statistically significant using the χ^2-square test and are designated as monomer (M) and early aggregates (A* and A).

concentration were also unable to accelerate the aggregation of Htt53Q *in vitro* (data not shown), suggesting that proline altered the aggregate core both *in vitro* and *in vivo*. This effect is solely due to changes in the aggregate structure by proline rather than any influence of the cellular constituents or the GFP tag in the *in vivo* experiments. The structure of the cellular GFP-Htt53Q aggregates was similar to that of the *in vitro* Htt53Q amyloids: both were ThT-positive and efficiently seeded the Htt53Q elongation *in vitro* (Figure 2D, Supporting Information Figure S5).

Aggregation of Htt exon 1 with an expanded polyQ stretch is a complex process, and various transient intermediate aggregate species (oligomers, protofibrils) can be formed in the reaction,[11,12] which are suggested to be the major cytotoxic culprits.[45] Proline altered the aggregation pathway when present throughout the aggregation process, and we anticipated that proline might destabilize these transient aggregates differently because of variations in the accessible protein surface (a combination of the accessible backbone and side chains). This raised the question as to whether proline could influence the early aggregation phases and thereby induce structural differences in the early aggregates and/or alternative species in the aggregation reaction. To address the early aggregation events of the Htt53Q aggregation, we used fluorescence correlation spectroscopy (FCS) in a single-molecule regime which avoids loss of information due to ensemble averaging that hinders resolving transiently coexisting populations. Fluorescently labeled and unlabeled Htt53Q were mixed (ratio 1:1000) to reduce fluorescence intensity during course of aggregation to only a few fluorescent monomers in each bulky species. The aggregation reaction was performed as the bulk studies and fibrils produced from this mixture were found by electron microscopy to be morphologically similar to the unlabeled Htt53Q fibrils; light scattering also confirmed identical aggregation kinetics (Supporting Information Figure S6). The Htt53Q autocorrelation curves shifted toward higher diffusion times as a function of the aggregation time, suggesting that at least two kinds of fluorescent particles with different mobility existed (Supporting Information Figure S7A). The appearance of the aggregates introduces high heterogeneity into the system which may exhibit anomalous diffusion and does not allow application of the two-component model for three-dimensional Brownian diffusion within a homogeneous fluid medium.[38] To determine population distributions without using a thermodynamic model, we extracted the first derivative of the individual autocorrelation functions and fit them to a Gaussian function (Figure 3A, Supporting Information Figure S7B). In the early phase of Htt53Q aggregation three different species could be identified: monomer (M) migrating with an average dwell time of 0.5 ms and two aggregate species passing the confocal volume with an average of 14 (A*) and 630 (A) ms (Figure 3A). The autocorrelation curves of the soluble Htt20Q showed a presence of only one species corresponding to the monomer throughout the time of measurements (data not shown), and a one-component fit was used for the G' function. For the aggregating Htt53Q we used a five-component model to fit the G' functions to the Gaussian function (Supporting Information Figure S7B). The presence of at least two well-distinguishable aggregate species A* and A and the small fractions of subpopulations of intermediate aggregates in the range of 10^0-10^2 ms (Supporting Information Figure S7B) suggest an incremental increase of the aggregate size in the course of aggregation; however, the FCS technique cannot resolve the steps of aggregate enlargement. For FCS to resolve multiple species the diffusion times must differ by a factor of ~1.6; i.e., the masses of the particles should differ by $\sim(1.6)^3$.[38] Strikingly, proline suppressed the accumulation of the A* assemblies; however, the larger A aggregates were built albeit with somewhat slowed kinetics (Figure 3B). The intensity of the A aggregates was significantly reduced over 120 min in the presence of proline; the origin of this effect, even though reproducible, is yet unclear.

The different physicochemical features of the assemblies grown in the presence of proline may also parallel alterations in the aggregate cytotoxicity. To evaluate the aggregate toxicity, we used a standardized approach:[46−48] preformed *in vitro* aggregates in the presence of proline were added to neuroblastoma N2a cells, and the cytotoxic effect was monitored by 3-(4,5-dimethylthiazol-2yl)-2,5-diphenyltetrazolium bromide (MTT) reduction assay. In agreement with previous studies,[49,50] a mixture of control Htt53Q protofibrils and fibrils grown without osmolytes caused a MTT reduction (~70%) indicative of cellular toxicity (Supporting Information Figure S8). Intriguingly, assemblies grown in the presence of proline showed no MTT reduction similar to control cells growing without aggregates (Supporting Information Figure S8), implying that aggregates assembled in the presence of proline were not toxic in cell-based assays.

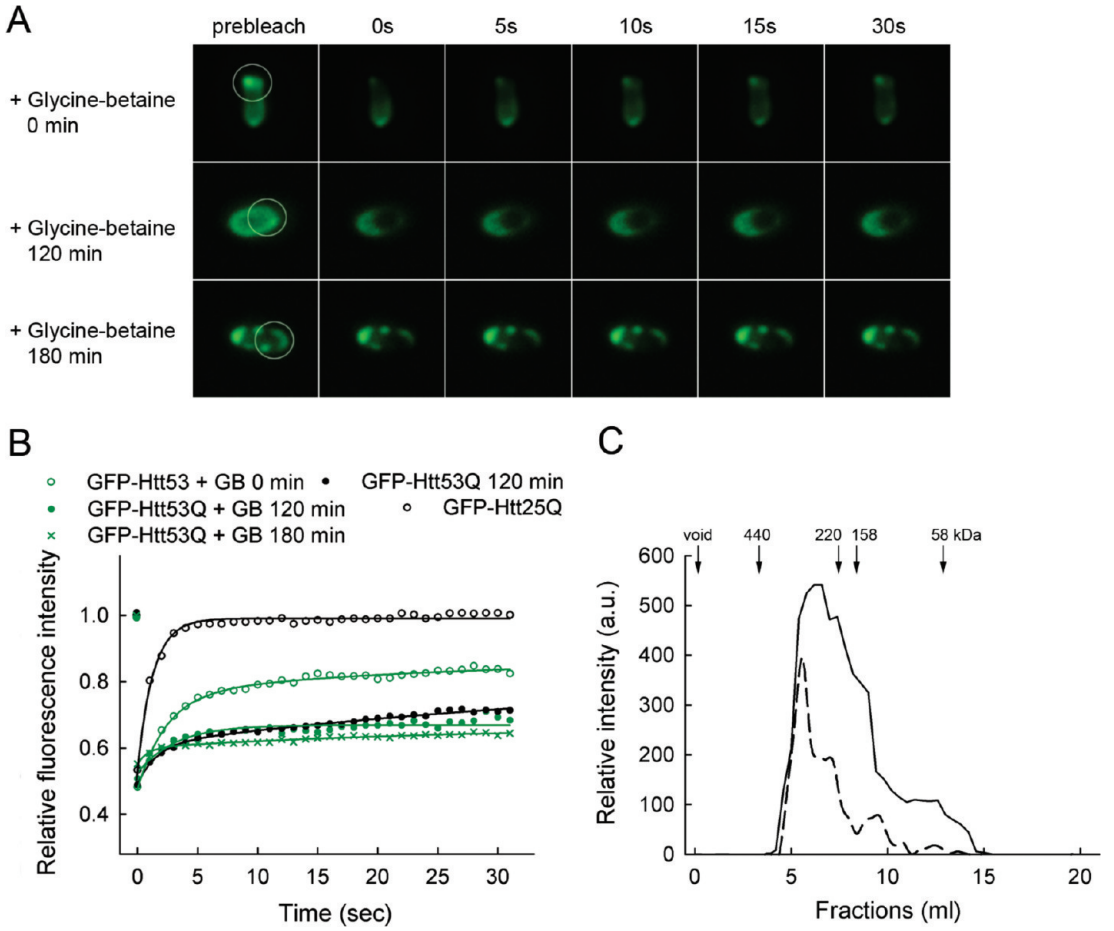

Figure 4. GB altered the mobility of Htt53Q and favored aggregation *in vivo*. (A) FRAP analysis of GFP-Htt53Q aggregates after internalization of GB in the cell at various times (times are indicated to the left of each FRAP-image series). (B) Quantitative analysis of the FRAP images. Solid lines represent a curve fit to a three-parameter single exponential or a five-parameter double exponential function. (C) GB increases the fraction of detergent-resistant GFP-Htt53Q aggregates. GB uptake was internalized concomitantly with aggregate induction (0 min as on the panel A), and intact GFP-Htt53Q aggregates grown in the presence of GB were fractionated into SDS-labile (solid) and SDS-resistant (dashed) species by size-exclusion chromatography. For further details see the legend to Figure 1.

Glycine−Betaine Acelerates PolyQ Aggregation both *in Vivo* and *in Vitro*. To compare the effect of other osmolytes on the Htt53Q aggregation, we examined GB, which is naturally enriched in the medulla of mammalian kidney to counteract urea stress.[43] In enteric bacteria GB is tranpsorted through the ProP and ProU transporers [51,52] and accumulates within few minutes [9] to concentrations similar to proline [53] provided that GB is available in the medium. GB exerted an opposite effect on the aggregate mobility to that observed with proline: When internalized in the cell at an intermediate stage of aggregation at which GFP-Htt53Q partitioned between detergent-resistant and SDS-labile aggregates (120 min, Figure 1C), GB markedly reduced the recovery and the mobility of the aggregates to 30% (Figure 4A,B, Table 1). GB did not alter the mobility of the late-stage Htt53Q aggregates (180 min, Table 1). Even when it was present throughout the aggregation cycle (0 min), the aggregates displayed only a partial recovery (Figure 4A,B) and mobility of 52% (Table 1) and partitioned between the SDS-labile and SDS-resistant fraction (Figure 4C).

In vivo GB accelerated the GFP-Htt53Q aggregation and the appearance of detergent-resistant immobile aggregates, and this effect could be recapitulated in *in vitro* experiments: GB accelerated the Htt53Q aggregation in a concentration-dependent fashion (Figure 5A), thereby forming aggregates with well-defined fibrillar phenotypes (Figure 5B). Similarly, in a concentration-dependent fashion glycine−betaine (GB) modulates the aggregation of a GST-GFP chimera into soluble or insoluble assemblies.[54] FCS measurements showed a very rapid formation of large aggregates early on (60 min) and whose large size reached the limitations of this technique (data not shown). Aggregates assembled in the presence of GB were able to seed the elongation of Htt53Q fibrils (Figure 5C) as efficiently as the control Htt53Q seeds (Figure 2D), implying similarities in the aggregate core of the fibrils grown with and without the osmolyte. When grown in the presence of GB the Htt53Q aggregates yielded a similar stability against thermal depolymerization as the control Htt53Q amyloid fibrils (Supporting Information Figure S9A). Adding GB at later time points stabilized the Htt53Q aggregates even more (Supporting Information Figure S9A), which remarkably paralleled the observations made *in vivo*. Intriguingly, addition of GB at the initiation of the Htt53Q aggregation caused an immediate rise in the ThT fluorescence without the apparent lag phase as opposed to the control Htt53Q aggregation (Supporting Information Figure S9B). Additionally, the early ThT-positive species that were formed in the lag-like phase of the aggregation reaction were seeding-competent species (Figure 5C), suggesting an early

dx.doi.org/10.1021/bi1018368 |*Biochemistry* 2011, 50, 2048–2060

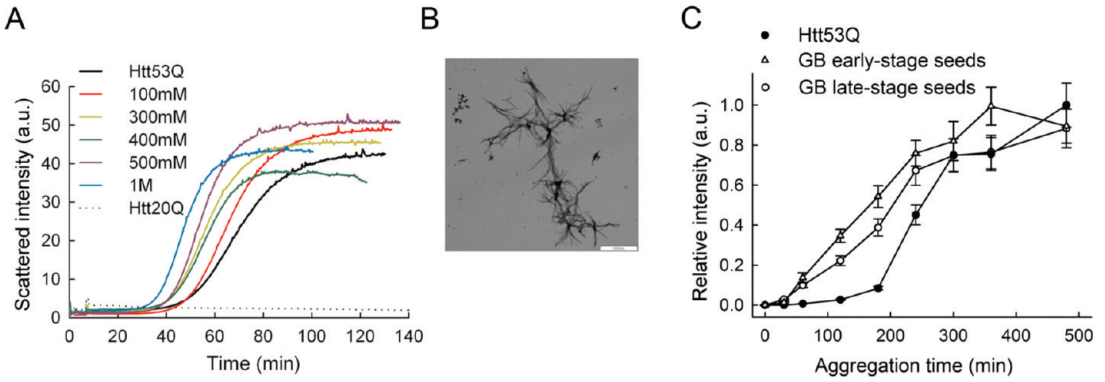

Figure 5. GB accelerated the aggregation of Htt53Q *in vitro*. (A) Aggregation kinetics of Htt53Q in the presence of different GB concentrations monitored by static light scattering. Htt20Q remained soluble throughout the time of analysis in the presence of GB. (B) Electron micrographs of the Htt53Q aggregates grown in the presence of GB for 24 h. Scale bar represents 1 μm; magnification 7777×. (C) Aggregates grown in the presence of GB accelerated the Htt53Q aggregation. The aggregation of Htt53Q in the presence of 0.5 M GB was allowed to proceed for 40 min (GB early-stage seeds; correspond to the end of the lag phase in panel A) or for 24 h (GB late-stage seeds), and the collected aggregates (10% (w/w)) were used to seed the *in vitro* aggregation reaction of Htt53Q and monitored by filter-retardation assay. Htt53Q denotes the *in vitro* aggregation kinetics of the unseeded control Htt53Q aggregation.

formation of the fibrillar aggregate core and absence of reaction intermediates.[55] Even though fibrillar aggregates were formed in the presence of GB, they did not exert any cytotoxic effect on the N2a cells (Supporting Information Figure S8).

TMAO Favors Formation of Bulky but Unstructured Aggregates. From the array of naturally occurring osmolytes, at high concentration TMAO exerts the strongest effect in inducing structure in naturally disordered proteins[56] and helps thermodynamically unstable proteins to fold.[57] Since the polyQ stretch of Htt exon 1 is intrinsically unstructured,[12] we reasoned that TMAO may stabilize Htt53Q and prevent it from aggregation. TMAO is not a natural osmolyte for *E. coli*, thus allowing only *in vitro* experiments. Intriguingly, TMAO markedly accelerated the Htt53Q aggregation (Figure 6A), thereby inducing the formation of unstructured, bulky, amorphous assemblies (Figure 6B) which exerted no cytotoxic effect (Supporting Information Figure S8). The effect of TMAO was strongly concentration-dependent (Figure 6A); the initial phase was shortened by increasing TMAO concentration. This concentration effect can be rationalized by the dominating osmophobic effect (i.e., unfavorable interactions with the peptide backbone) for this osmolyte.[23] Interestingly, in the context of aggregation of natively disordered α-synuclein TMAO shows concentration-dependent effects: at moderate concentration it populates an aggregation-prone intermediate with strong propensity to form fibrillar species, whereas higher concentrations induce tight structuring of the monomer which further self-assembles into oligomers.[56] Unlike the amorphous aggregates formed in the presence of proline, the Htt53Q aggregates were extremely stable against thermal depolymerization in the presence of TMAO exceeding even the stability of the control Htt53Q fibrils (Figure 6C). Strikingly, though with no apparent fibrillar phenotype, the aggregates formed in the presence of TMAO were partially SDS-resistant (Supporting Information Figure S10A). However, their core structure differed from that of the Htt53Q fibrils since they were incapable of seeding the Htt53Q elongation *in vitro* (Supporting Information Figure S10B). FCS measurements showed that TMAO introduced a broad fraction of aggregates with large variations in diffusion properties early in the aggregation, as indicated by the broadening and partial overlapping of the distribution of the three main species (30 and 60 min, Figure 6D). Consequently, these broad ensembles of aggregates are further packed into tight and bulky assemblies. TMAO is rapidly excluded from protein surfaces,[23,58] which provides the molecular explanation for the observed rapid formation of bulky amorphous aggregates: the aggregates sequester maximum surface area and thereby diminish the contact with the osmolyte.

DISCUSSION

The propensity of a protein to aggregate is an intrinsic feature of the protein sequence and is influenced critically by the solvent environment.[59] In this study, we analyzed the impact of three osmoprotectants, which maintain the solvent composition in the cell in response to external stress, on the fibrillization of exon 1 of Htt with an expanded polyQ stretch (here, the number of glutamine residues is 53) implicated in the Huntington's disease pathology. Our results establish that these three osmolytes differently modulated the polyQ aggregation, and their effect can be summarized as follows (Figure 7): (i) *Proline* disfavors the fibrillization by populating the monomer and inducing the formation of alternative aggregates with amorphous phenotype, (ii) *GB* in contrast favors the fibrillization, and (iii) *TMAO* alters the aggregation pathway and leads to rapid formation of amorphous aggregates. Proline and TMAO showed similar outcomes; i.e., amorphous aggregates are formed in the presence of both osmolytes; however, their molecular mode of action is somewhat opposite. The effect of TMAO is strongly concentration-dependent whereas proline shows only a weak concentration dependence. Gln is the dominating amino acid in the Htt53Q protein representing 49% of the side chains in Htt53Q. The free energy of Gln side chains and backbone transfer from water to osmolytes determined by Auton and Bolen[23] provides the molecular rationale for the variations we observed. By TMAO, the most effective protecting osmolyte, the preferential exclusion of 1M solute from the peptide backbone (87 cal·mol^{-1}) and the Gln side chain (41.4 cal·mol^{-1})[23,60,61] triggers the rapid collapse of Htt53Q monomers into highly stable, bulky amorphous aggregates. Although unstructured, these aggregates sequester a large backbone surface area which decreases the unfavorable interactions with the solute. Proline is a weakly stabilizing osmolyte by which the osmophobic effect on the backbone (33.5 cal·mol^{-1})

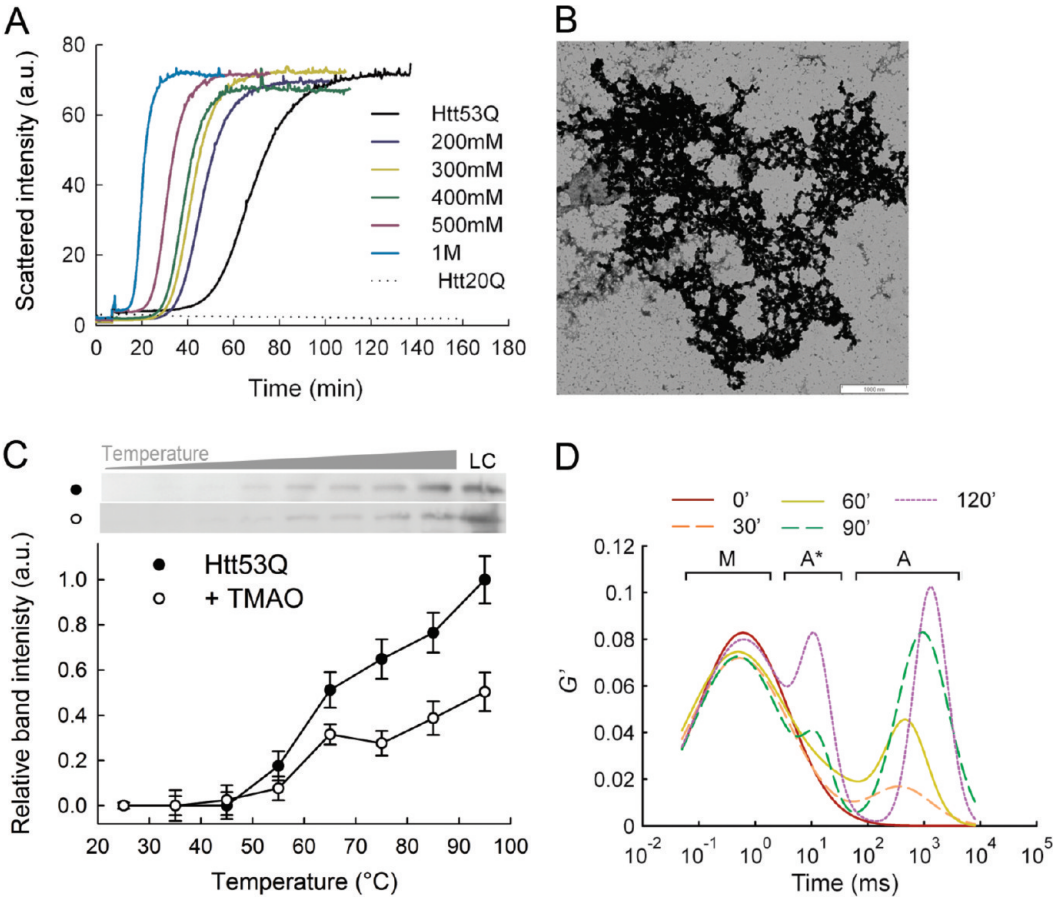

Figure 6. TMAO caused a fast collapse of Htt53Q into unstructured aggregates. (A) Aggregation kinetics of Htt53Q in the presence of different TMAO concentrations monitored by static light scattering. The nonaggregating Htt20Q protein was not influenced by addition of TMAO. (B) Electron micrographs of the Htt53Q aggregates grown in the presence of 0.5 M TMAO for 24 h. Scale bar represents 1 μm; magnification 12000×. (C) Htt53Q aggregates assembled in the presence of TMAO were less susceptible to thermal depolymerization than the Htt53Q fibrils grown without osmolyte. (D) FCS measurements of the early stages of the Htt53Q aggregation in the presence of 0.5 M TMAO. For details on the labeling refer to Figure 3.

only slightly dominates over the favorable interactions with the Gln side chains (-32 cal·mol^{-1}) only.[23,60,61] The competition between solvophobic backbone interactions will favor formation of aggregate assemblies with reduced solvent-accessible backbone surface; in parallel, the favorable interactions with the Gln side chains solubilize the Htt53Q monomer and reduce the aggregation rates.

GB is the only osmolyte that enhances fibrillogenesis, and the effect is strongly concentration-dependent. Its effect can be rationalized by the additive effect of the preferential exclusion of 1M GB from the backbone (62 cal·mol^{-1}) and the mild exclusion from the Gln side chain (7.6 cal·mol^{-1}).[23,60,61] Considering the backbone as a major determinant of the aggregate morphology, one would expect that in the presence of GB Htt53Q would assemble into amorphous aggregates which have an intermediate free energy of backbone transfer from water to 1M osmolyte compared to the other two osmolytes (cal·mol^{-1}: 87 for TMAO vs 62 for GB vs 33 for proline).[60] GB, however, favored formation of fibrillar aggregates whose phenotype can be explained with the variations in the transfer free energies of Gln side chains: GB is very mildly excluded from the Gln side chain (7.6 cal·mol^{-1}), indicating little to no changes of Gln solvation by water or by GB. Consequently, aggregates with similar morphology to the control Htt53Q assemblies in buffer are formed in the presence of GB. Supportive for this conclusion is the fact that in presence of glycerol fibrillar phenotype is accessible for Htt53Q (data now shown). Glycerol, similarly to GB, is mildly excluded from the Gln side chain. Although a fibrillar phenotype is accessible in the presence of this solute, we propose that GB is also protective: Its effect is reminiscent of the aggregation pathway of functional amyloids whose fast, template-assisted polymerization avoids the formation of intermediate aggregates with toxic properties.[62] In the presence of GB, species with a fibrillar aggregate core were formed early in the aggregation reaction (i.e, in the lag-like phase) implying that GB accelerates the Htt53Q fibrillization most likely by bypassing the formation of any intermediate species. Consistent with the protective role of the large inclusions, a recent paper by Bodner et al. demonstrates that chemical compounds promoting inclusion formation decrease the toxic effects of Huntington's and Parkinson's diseases in human neuroglioma cells,[63] suggesting that an osmolyte that mimics the pathway of fibrillization of a functional amyloid could be a promising strategy to ameliorate the toxicity in pathological amyloidogenesis.

Amyloid pathways can be modulated by molecular chaperones[64,65] and small pharmacological molecules.[63,66−68] In both cases, there is a mechanistic similarity in the effect on polyQ amyloidogenesis; they modulate the amyloidogenity by either introducing a

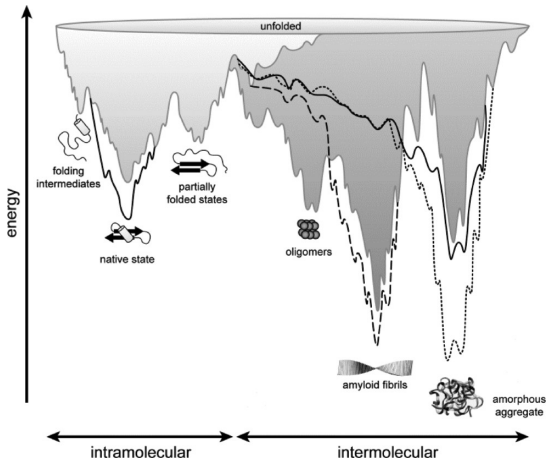

Figure 7. Model of the effect of osmolytes on the energy landscape of the Htt exon 1 fibrillogenesis. Proline (black line) stabilizes the native monomer and introduces an alternative branch to the aggregation pathway leading to the formation of off-pathway amorphous aggregates. Similarly, TMAO (dotted line) also induces the formation of off-pathway amorphous aggregates with a much higher thermodynamic stability than the fibrils. The amyloid fibrils are only accessible in the presence of GB (dashed line) which accelerates the aggregation, most likely without formation of any aggregation intermediates (i.e., oligomers). The grid of the combined landscape of folding (light gray) and aggregation (dark gray) reactions is discussed elsewhere.[69,70]

nontoxic, nonamyloidogenic branch into the aggregation pathway or enhancing the aggregation. There are certain limitations to both approaches: to specifically target overexpression of the molecular chaperones in damaged cells only, while administration of small molecules into the body's fluids would encounter some stability and diffusion limitations. In contrast, the osmocompensatory response is an evolutionary-optimized strategy to combat volume changes, and the osmolytes can be upregulated in virtually any type of cell. As a natural mechanism, compatible osmolytes overcome potential interference with other cellular functions. Cell volume perturbations are challenges for cells in animal organs, with particularly dramatic consequences in the brain. Accordingly, neuronal cells, which are the cellular medium of the polyQ pathologies, employ a large variety of osmolytes (i.e., amino acids, organic acids, amides, and sugars) to maintain cell volume homeostasis.[43] Coupling the stress response to modulate the aggregation pathway provides a molecular rationale to design applications of osmolytes for biomedical therapies of degenerative neuropathologies. Most importantly, the differential impact of the osmolytes on the various aggregate species allows for design of strategies to modulate the aggregation pathways at different stages.

■ ASSOCIATED CONTENT

Supporting Information. Detailed results on *in vivo* aggregation and expression (Figures S1 and S2), kinetics of PreScission cleavage (Figure S3), kinetics of aggregation in the presence of various osmolytes monitored by ThT fluorescence and stability against thermal depolymerization (Figures S4, S5, and S9), seeding kinetics (Figure S10), toxicity assays (Figure S8), the effect of monomer labeling on the aggregation (Figure S6), and exemplary FCS curves and their Gaussian fits (Figure S7). This material is available free of charge via the Internet at http://pubs.acs.org.

■ AUTHOR INFORMATION

Corresponding Author

*E-mail: ignatova@uni-potsdam.de. Tel: 49-331-977-5130. Fax: 49-331-997-5128.

Funding Sources

This work was supported by the SysMO (Kosmobac project) and DFG (IG73/8-1) grants to Z.I.

■ ACKNOWLEDGMENT

We are grateful to Bert Poolman (University of Groningen) for the suggestion to use the first derivative in the quantification of the FCS analysis and to Sam Miller (University of Aberdeen) and K. Gast (University of Potsdam) for the fruitful comments on the manuscript. We thank B. Tiersch and J. Koetz (University of Potsdam) for the electron microscopy images. The monoclonal MW1 and MW8 antibodies developed by J. Ko and P. Patterson were obtained from the Developmental Studies Hybridoma Bank (University of Iowa).

■ ABBREVIATIONS

GB, glycine−betaine; FCS, fluorescence correlation spectroscopy; FRAP, fluorescence recovery after photobleaching; GFP, green fluorescent protein; GST, gluthatione *S*-tranferase; Htt, huntingtin; IPTG, isopropyl β-D-thiogalactoside; TMAO, trimethylamine *N*-oxide.

■ REFERENCES

(1) Diamant, S., Eliahu, N., Rosenthal, D., and Goloubinoff, P. (2001) Chemical chaperones regulate molecular chaperones in vitro and in cells under combined salt and heat stresses. *J. Biol. Chem. 276*, 39586–39591.

(2) Bolen, D. W., and Rose, G. D. (2008) Structure and energetics of the hydrogen-bonded backbone in protein folding. *Annu. Rev. Biochem. 77*, 339–362.

(3) Hoffmann, E. K., Lambert, I. H., and Pedersen, S. F. (2009) Physiology of cell volume regulation in vertebrates. *Physiol. Rev. 89*, 193–277.

(4) Yancey, P. H. (2005) Organic osmolytes as compatible, metabolic and counteracting cytoprotectants in high osmolarity and other stresses. *J. Exp. Biol. 208*, 2819–2830.

(5) Street, T. O., Bolen, D. W., and Rose, G. D. (2006) A molecular mechanism for osmolyte-induced protein stability. *Proc. Natl. Acad. Sci. U.S.A. 103*, 13997–14002.

(6) Lamitina, T., Huang, C. G., and Strange, K. (2006) Genome-wide RNAi screening identifies protein damage as a regulator of osmoprotective gene expression. *Proc. Natl. Acad. Sci. U.S.A. 103*, 12173–12178.

(7) Wood, J. M. (1999) Osmosensing by bacteria: signals and membrane-based sensors. *Microbiol. Mol. Biol. Rev. 63*, 230–262.

(8) Cayley, S., and Record, M. T., Jr. (2003) Roles of cytoplasmic osmolytes, water, and crowding in the response of *Escherichia coli* to osmotic stress: biophysical basis of osmoprotection by glycine betaine. *Biochemistry 42*, 12596–12609.

(9) Koo, S. P., Higgins, C. F., and Booth, I. R. (1991) Regulation of compatible solute accumulation in *Salmonella typhimurium*: evidence for a glycine betaine efflux system. *J. Gen. Microbiol. 137*, 2617–2625.

(10) Ross, C. A., and Poirier, M. A. (2004) Protein aggregation and neurodegenerative disease. *Nat. Med. 10* (Suppl.), S10–S17.

(11) Poirier, M. A., Li, H., Macosko, J., Cai, S., Amzel, M., and Ross, C. A. (2002) Huntingtin spheroids and protofibrils as precursors in polyglutamine fibrilization. *J. Biol. Chem. 277*, 41032–41037.

(12) Thakur, A. K., Jayaraman, M., Mishra, R., Thakur, M., Chellgren, V. M., Byeon, I. J., Anjum, D. H., Kodali, R., Creamer, T. P., Conway, J. F., Gronenborn, A. M., and Wetzel, R. (2009) Polyglutamine disruption of the

huntingtin exon 1 N terminus triggers a complex aggregation mechanism. *Nat. Struct. Mol. Biol. 16*, 380–389.

(13) Behrends, C., Langer, C. A., Boteva, R., Bottcher, U. M., Stemp, M. J., Schaffar, G., Rao, B. V., Giese, A., Kretzschmar, H., Siegers, K., and Hartl, F. U. (2006) Chaperonin TRiC promotes the assembly of polyQ expansion proteins into nontoxic oligomers. *Mol. Cell 23*, 887–897.

(14) Kim, S., Nollen, E. A., Kitagawa, K., Bindokas, V. P., and Morimoto, R. I. (2002) Polyglutamine protein aggregates are dynamic. *Nat. Cell Biol. 4*, 826–831.

(15) Cowan, K. J., Diamond, M. I., and Welch, W. J. (2003) Polyglutamine protein aggregation and toxicity are linked to the cellular stress response. *Hum. Mol. Genet. 12*, 1377–1391.

(16) Chun, W., Lesort, M., Lee, M., and Johnson, G. V. (2002) Transient osmotic stress facilitates mutant huntingtin aggregation. *Neuroreport 13*, 2543–2546.

(17) Miyata, R., Hayashi, M., Tanuma, N., Shioda, K., Fukatsu, R., and Mizutani, S. (2008) Oxidative stress in neurodegeneration in dentatorubral-pallidoluysian atrophy. *J. Neurol. Sci. 264*, 133–139.

(18) Reina, C. P., Zhong, X., and Pittman, R. N. (2010) Proteotoxic stress increases nuclear localization of ataxin-3. *Hum. Mol. Genet. 19*, 235–249.

(19) Duennwald, M. L., Jagadish, S., Muchowski, P. J., and Lindquist, S. (2006) Flanking sequences profoundly alter polyglutamine toxicity in yeast. *Proc. Natl. Acad. Sci. U.S.A. 103*, 11045–11050.

(20) Tam, S., Spiess, C., Auyeung, W., Joachimiak, L., Chen, B., Poirier, M. A., and Frydman, J. (2009) The chaperonin TRiC blocks a huntingtin sequence element that promotes the conformational switch to aggregation. *Nat. Struct. Mol. Biol. 16*, 1279–1285.

(21) Bevivino, A. E., and Loll, P. J. (2001) An expanded glutamine repeat destabilizes native ataxin-3 structure and mediates formation of parallel beta -fibrils. *Proc. Natl. Acad. Sci. U.S.A. 98*, 11955–11960.

(22) Ignatova, Z., and Gierasch, L. M. (2006) Extended polyglutamine tracts cause aggregation and structural perturbation of an adjacent beta barrel protein. *J. Biol. Chem. 281*, 12959–12967.

(23) Auton, M., and Bolen, D. W. (2005) Predicting the energetics of osmolyte-induced protein folding/unfolding. *Proc. Natl. Acad. Sci. U.S.A. 102*, 15065–15068.

(24) Tanaka, M., Machida, Y., Niu, S., Ikeda, T., Jana, N. R., Doi, H., Kurosawa, M., Nekooki, M., and Nukina, N. (2004) Trehalose alleviates polyglutamine-mediated pathology in a mouse model of Huntington disease. *Nat. Med. 10*, 148–154.

(25) Furusho, K., Yoshizawa, T., and Shoji, S. (2005) Ectoine alters subcellular localization of inclusions and reduces apoptotic cell death induced by the truncated Machado-Joseph disease gene product with an expanded polyglutamine stretch. *Neurobiol. Dis. 20*, 170–178.

(26) Sarkar, S., Davies, J. E., Huang, Z., Tunnacliffe, A., and Rubinsztein, D. C. (2007) Trehalose, a novel mTOR-independent autophagy enhancer, accelerates the clearance of mutant huntingtin and alpha-synuclein. *J. Biol. Chem. 282*, 5641–5652.

(27) Racher, K. I., Culham, D. E., and Wood, J. M. (2001) Requirements for osmosensing and osmotic activation of transporter ProP from *Escherichia coli*. *Biochemistry 40*, 7324–7333.

(28) Lippincott-Schwartz, J., Snapp, E., and Kenworthy, A. (2001) Studying protein dynamics in living cells. *Nat. Rev. Mol. Cell. Biol. 2*, 444–456.

(29) Stenoien, D. L., Mielke, M., and Mancini, M. A. (2002) Intranuclear ataxin1 inclusions contain both fast- and slow-exchanging components. *Nat. Cell Biol. 4*, 806–810.

(30) Wanker, E. E., Scherzinger, E., Heiser, V., Sittler, A., Eickhoff, H., and Lehrach, H. (1999) Membrane filter assay for detection of amyloid-like polyglutamine-containing protein aggregates. *Methods Enzymol. 309*, 375–386.

(31) Ko, J., Ou, S., and Patterson, P. H. (2001) New anti-huntingtin monoclonal antibodies: implications for huntingtin conformation and its binding proteins. *Brain Res. Bull. 56*, 319–329.

(32) Scherzinger, E., Sittler, A., Schweiger, K., Heiser, V., Lurz, R., Hasenbank, R., Bates, G. P., Lehrach, H., and Wanker, E. E. (1999) Self-assembly of polyglutamine-containing huntingtin fragments into amyloid-like fibrils: implications for Huntington's disease pathology. *Proc. Natl. Acad. Sci. U.S.A. 96*, 4604–4609.

(33) Chien, P., DePace, A. H., Collins, S. R., and Weissman, J. S. (2003) Generation of prion transmission barriers by mutational control of amyloid conformations. *Nature 424*, 948–951.

(34) Nekooki-Machida, Y., Kurosawa, M., Nukina, N., Ito, K., Oda, T., and Tanaka, M. (2009) Distinct conformations of in vitro and in vivo amyloids of huntingtin-exon1 show different cytotoxicity. *Proc. Natl. Acad. Sci. U.S.A. 106*, 9679–9684.

(35) Legleiter, J., Lotz, G. P., Miller, J., Ko, J., Ng, C., Williams, G. L., Finkbeiner, S., Patterson, P. H., and Muchowski, P. J. (2009) Monoclonal antibodies recognize distinct conformational epitopes formed by polyglutamine in a mutant huntingtin fragment. *J. Biol. Chem. 284*, 21647–21658.

(36) Munishkina, L. A., Phelan, C., Uversky, V. N., and Fink, A. L. (2003) Conformational behavior and aggregation of alpha-synuclein in organic solvents: modeling the effects of membranes. *Biochemistry 42*, 2720–2730.

(37) Ignatova, Z., Thakur, A. K., Wetzel, R., and Gierasch, L. M. (2007) In-cell aggregation of a polyglutamine-containing chimera is a multistep process initiated by the flanking sequence. *J. Biol. Chem. 282*, 36736–36743.

(38) Chen, H., Farkas, E. R., and Webb, W. W. (2008) Chapter 1: in vivo applications of fluorescence correlation spectroscopy. *Methods Cell Biol. 89*, 3–35.

(39) Li, X. J., Li, S. H., Sharp, A. H., Nucifora, F. C., Jr., Schilling, G., Lanahan, A., Worley, P., Snyder, S. H., and Ross, C. A. (1995) A huntingtin-associated protein enriched in brain with implications for pathology. *Nature 378*, 398–402.

(40) de Groot, N. S., Sabate, R., and Ventura, S. (2009) Amyloids in bacterial inclusion bodies. *Trends Biochem. Sci. 34*, 408–416.

(41) Jebbar, M., Talibart, R., Gloux, K., Bernard, T., and Blanco, C. (1992) Osmoprotection of *Escherichia coli* by ectoine: uptake and accumulation characteristics. *J. Bacteriol. 174*, 5027–5035.

(42) Dinnbier, U., Limpinsel, E., Schmid, R., and Bakker, E. P. (1988) Transient accumulation of potassium glutamate and its replacement by trehalose during adaptation of growing cells of *Escherichia coli* K-12 to elevated sodium chloride concentrations. *Arch. Microbiol. 150*, 348–357.

(43) Burg, M. B., and Ferraris, J. D. (2008) Intracellular organic osmolytes: function and regulation. *J. Biol. Chem. 283*, 7309–7313.

(44) Chien, P., and Weissman, J. S. (2001) Conformational diversity in a yeast prion dictates its seeding specificity. *Nature 410*, 223–227.

(45) Ross, C. A., and Poirier, M. A. (2005) Opinion: what is the role of protein aggregation in neurodegeneration? *Nat. Rev. Mol. Cell Biol. 6*, 891–898.

(46) Bucciantini, M., Giannoni, E., Chiti, F., Baroni, F., Formigli, L., Zurdo, J., Taddei, N., Ramponi, G., Dobson, C. M., and Stefani, M. (2002) Inherent toxicity of aggregates implies a common mechanism for protein misfolding diseases. *Nature 416*, 507–511.

(47) Ren, P. H., Lauckner, J. E., Kachirskaia, I., Heuser, J. E., Melki, R., and Kopito, R. R. (2009) Cytoplasmic penetration and persistent infection of mammalian cells by polyglutamine aggregates. *Nat. Cell Biol. 11*, 219–225.

(48) Shearman, M. S. (1999) Toxicity of protein aggregates in PC12 cells: 3-(4,5-dimethylthiazol-2-yl)-2,5-diphenyltetrazolium bromide assay. *Methods Enzymol. 309*, 716–723.

(49) Colby, D. W., Chu, Y., Cassady, J. P., Duennwald, M., Zazulak, H., Webster, J. M., Messer, A., Lindquist, S., Ingram, V. M., and Wittrup, K. D. (2004) Potent inhibition of huntingtin aggregation and cytotoxicity by a disulfide bond-free single-domain intracellular antibody. *Proc. Natl. Acad. Sci. U.S.A. 101*, 17616–17621.

(50) Tsirigotis, M., Baldwin, R. M., Tang, M. Y., Lorimer, I. A., and Gray, D. A. (2008) Activation of p38MAPK contributes to expanded polyglutamine-induced cytotoxicity. *PLoS One 3*, e2130.

(51) Cairney, J., Booth, I. R., and Higgins, C. F. (1985) Osmoregulation of gene expression in *Salmonella typhimurium*: proU encodes an osmotically induced betaine transport system. *J. Bacteriol. 164*, 1224–1232.

(52) Cairney, J., Booth, I. R., and Higgins, C. F. (1985) *Salmonella typhimurium* proP gene encodes a transport system for the osmoprotectant betaine. *J. Bacteriol. 164*, 1218–1223.

(53) Record, M. T., Jr., Courtenay, E. S., Cayley, S., and Guttman, H. J. (1998) Biophysical compensation mechanisms buffering *E. coli* protein-nucleic acid interactions against changing environments. *Trends Biochem. Sci. 23*, 190–194.

(54) Natalello, A., Liu, J., Ami, D., Doglia, S. M., and de Marco, A. (2009) The osmolyte betaine promotes protein misfolding and disruption of protein aggregates. *Proteins 75*, 509–517.

(55) Chen, S., Ferrone, F. A., and Wetzel, R. (2002) Huntington's disease age-of-onset linked to polyglutamine aggregation nucleation. *Proc. Natl. Acad. Sci. U.S.A. 99*, 11884–11889.

(56) Uversky, V. N., Li, J., and Fink, A. L. (2001) Trimethylamine-N-oxide-induced folding of alpha-synuclein. *FEBS Lett. 509*, 31–35.

(57) Scaramozzino, F., Peterson, D. W., Farmer, P., Gerig, J. T., Graves, D. J., and Lew, J. (2006) TMAO promotes fibrillization and microtubule assembly activity in the C-terminal repeat region of tau. *Biochemistry 45*, 3684–3691.

(58) Kita, Y., Arakawa, T., Lin, T. Y., and Timasheff, S. N. (1994) Contribution of the surface free energy perturbation to protein-solvent interactions. *Biochemistry 33*, 15178–15189.

(59) Dobson, C. M. (2003) Protein folding and misfolding. *Nature 426*, 884–890.

(60) Auton, M., and Bolen, D. W. (2004) Additive transfer free energies of the peptide backbone unit that are independent of the model compound and the choice of concentration scale. *Biochemistry 43*, 1329–1342.

(61) Auton, M., Bolen, D. W., and Rosgen, J. (2008) Structural thermodynamics of protein preferential solvation: osmolyte solvation of proteins, amino acids, and peptides. *Proteins 73*, 802–813.

(62) Fowler, D. M., Koulov, A. V., Alory-Jost, C., Marks, M. S., Balch, W. E., and Kelly, J. W. (2006) Functional amyloid formation within mammalian tissue. *PLoS Biol. 4*, e6.

(63) Bodner, R. A., Outeiro, T. F., Altmann, S., Maxwell, M. M., Cho, S. H., Hyman, B. T., McLean, P. J., Young, A. B., Housman, D. E., and Kazantsev, A. G. (2006) Pharmacological promotion of inclusion formation: a therapeutic approach for Huntington's and Parkinson's diseases. *Proc. Natl. Acad. Sci. U.S.A. 103*, 4246–4251.

(64) Cohen, F. E., and Kelly, J. W. (2003) Therapeutic approaches to protein-misfolding diseases. *Nature 426*, 905–909.

(65) Muchowski, P. J., and Wacker, J. L. (2005) Modulation of neurodegeneration by molecular chaperones. *Nat. Rev. Neurosci. 6*, 11–22.

(66) Arakawa, T., Ejima, D., Kita, Y., and Tsumoto, K. (2006) Small molecule pharmacological chaperones: From thermodynamic stabilization to pharmaceutical drugs. *Biochim. Biophys. Acta 1764*, 1677–1687.

(67) Desai, U. A., Pallos, J., Ma, A. A., Stockwell, B. R., Thompson, L. M., Marsh, J. L., and Diamond, M. I. (2006) Biologically active molecules that reduce polyglutamine aggregation and toxicity. *Hum. Mol. Genet. 15*, 2114–2124.

(68) Ehrnhoefer, D. E., Duennwald, M., Markovic, P., Wacker, J. L., Engemann, S., Roark, M., Legleiter, J., Marsh, J. L., Thompson, L. M., Lindquist, S., Muchowski, P. J., and Wanker, E. E. (2006) Green tea (−)-epigallocatechin-gallate modulates early events in huntingtin misfolding and reduces toxicity in Huntington's disease models. *Hum. Mol. Genet. 15*, 2743–2751.

(69) Clark, P. L. (2004) Protein folding in the cell: reshaping the folding funnel. *Trends Biochem. Sci. 29*, 527–534.

(70) Jahn, T. R., and Radford, S. E. (2005) The Yin and Yang of protein folding. *FEBS J. 272*, 5962–5970.